Simulation of Large Spatial Domain Ultrasound Scattering Problems

Erwin J. Alles, Koen W.A. van Dongen
Laboratory of Acoustical Imaging and Sound Control
Delft University of Technology, The Netherlands
Email: E.J.Alles@tudelft.nl, K.W.A.vanDongen@tudelft.nl

Abstract

Currently, many ultrasound simulations of medical imaging modalities, like IntraVascular UltraSound (IVUS) are performed using the Field II software. This software models scattering bodies as collections of point-scatterers and evaluates the resulting total pressure field within the Born approximation. Consequently, it assumes a constant speed of sound throughout the volume. Therefore, modeled reflections arrive at incorrect times, and errors are introduced if thickness measurements are performed from simulated data. In addition, multiple scattering is neglected in this approximation, which means that for strong contrasts results obtained with Field II are incomplete.

To circumvent these issues, we have developed software which efficiently computes the total pressure field within a volume due to scattering off contrasts of arbitrary shape and magnitude. The software uses a conjugate gradient (CG) scheme to solve, in the temporal Laplace domain, the scatter integral equation for the total field, given known sources and contrasts. Spatial domain decomposition is used to allow for large domains of which the memory load would otherwise exceed the amount of memory present in current machines. To avoid reflections on domain boundaries, Perfectly Matched Layers (PMLs) are applied in the temporal Laplace domain.

We will compare the simulated received signals, using both programs, for an acoustic probe measuring plaque thickness in an artery and show that our software yields better results in certain situations compared to results obtained with the Field II software.

Introduction

IntraVascular UltraSound (IVUS) is a medical imaging modality aimed at detecting atherosclerotic plaque [1]. With IVUS, a catheter containing an ultrasound probe is positioned into the vascular system which transmits ultrasound pulses and measures the reflected wavefield. From these reflections, information about the properties of the insonified tissue is obtained.

To improve the quality of current IVUS systems, and ultrasound imaging systems in general, high-quality numerical simulations of pulse echo signals scattered off digital phantoms are required. Currently, many simulations are performed using the Field II software [2, 3], both for IVUS and other imaging modalities (e.g. [4, 5, 6]). This software is widely used, tested against measurements and even used as validation for other simulation tools [7].

However, Field II calculates transmitted and received pressures within the Born approximation only. Therefore, the speed of sound is constant throughout the modeled volume, and consequently propagation times will not be predicted correctly. This leads to errors when the thickness of layers is to be determined. In addition, multiple scattering is not accounted for, so in some situations the synthetic data is incomplete. This plays an important role in e.g. ultrasound carotid artery imaging [8], as reverberation deteriorates the image quality.

To circumvent these issues, we have developed software which, in the temporal Laplace domain, computes the convolutional scatter equation, for known incident field and known contrast function, beyond the Born approximation using a Conjugate Gradient (CG) scheme. To limit computational and memory loads, domain decomposition and Perfectly Matched Layers (PMLs) are applied.

In this paper, first the theory will be treated, followed by its implementation. Then comparisons between our software and Field II are made for situations found in IVUS which are commonly modeled with Field II. Finally conclusions will be drawn.

Theory

Integral Equation

The scatter problem is described by the convolutional integral equation, of which the derivation can be found in e.g. [9],

$$\begin{aligned} \widehat{p}^{\,\mathrm{inc}}(\vec{r}) &= \widehat{p}^{\,\mathrm{tot}}(\vec{r}) \\ &- \widehat{G}(\vec{r},\vec{r}') * \left[\widehat{k}_0^2 X^{\kappa}(\vec{r}')\widehat{p}^{\,\mathrm{tot}}(\vec{r}')\right] \\ &- \widehat{G}(\vec{r},\vec{r}') * \left[\vec{\nabla}\cdot X^{\rho}(\vec{r}')\vec{\nabla}\widehat{p}^{\,\mathrm{tot}}(\vec{r}')\right]. \end{aligned} \tag{1}$$

In this equation, $\widehat{p}^{\,\mathrm{inc}}(\vec{r})$ denotes the known incident pressure field in the frequency domain generated by the transducer, and $\widehat{G}(\vec{r},\vec{r}')$ the Green's function for a homogeneous background medium, which is obtained by solving the Helmholtz equation for a three-dimensional Dirac distribution. $\widehat{k}_0 = \frac{\omega}{c}$ is the wavenumber in the background medium, $X^{\kappa}(\vec{r}) \equiv \frac{\kappa^{\mathrm{scat}}(\vec{r})-\kappa^{\mathrm{bg}}}{\kappa^{\mathrm{bg}}}$ the contrast in compressibility κ, $X^{\rho}(\vec{r}) \equiv \frac{\rho^{\mathrm{bg}}-\rho^{\mathrm{scat}}(\vec{r})}{\rho^{\mathrm{scat}}(\vec{r})}$ the contrast in volume density of mass ρ, and $\widehat{p}^{\,\mathrm{tot}}(\vec{r})$ the unknown total pressure field. Superscripts "bg" and "scat" indicate material properties of the background medium and the scattering body, respectively. The symbols $*$, $\vec{\nabla}$ and

· indicate a three-dimensional spatial convolution, the gradient operator and an inner product, respectively.

Solution Method

For known incident field and contrasts, the linear integral equation (1) is solved by inverting the convolution operator on a discrete grid. Directly inverting this operator is, for large domains, not possible due to memory- and computation time restrictions. Therefore, the integral equation will be solved iteratively using a CG scheme because of its flexibility and guaranteed convergence. More specific, we use the Bi-CGSTAB scheme [10] for its fast convergence and simplicity.

Observing equation (1) reveals that discretization of the equation is not trivial. Firstly, to overcome problems associated with the singularity of the Green's function we use its weak form [11].

Secondly, spatial derivatives have to be taken of discontinuous functions, and therefore cannot be taken in the spatial Laplace domain. To improve on accuracy, a symmetric 17-point stencil is used,

$$\frac{\partial f}{\partial x} \approx [a_1 a_2 \dots a_8] \cdot \begin{bmatrix} f(x+\Delta x) - f(x-\Delta x) \\ f(x+2\Delta x) - f(x-2\Delta x) \\ \vdots \\ f(x+8\Delta x) - f(x-8\Delta x) \end{bmatrix} \quad (2)$$

where the constants $a_1, a_2, \dots, a_8$ are found by Taylor expanding $f(x)$ around x.

Thirdly, the spatial convolution is a computationally expensive operator. To reduce the computational load, the convolution is computed in the spatial Laplace domain using FFT's, at the expense of an increase in memory load.

Perfectly Matched Layers

Any numerical grid will have finite dimensions. Consequently, if the boundaries of the domain are not free from contrasts, additional scattering off the domain boundaries will occur, which has to be suppressed. This is achieved by attenuating the waves propagating towards the domain boundaries in an absorbing layer. To avoid reflection off this absorbing layer while keeping the absorbing layers relatively thin, we have applied Perfectly Matched Layers (PMLs) [12] in the frequency domain. Using layers of only a few wavelengths thick, virtually no reflections occur off the domain boundaries and the PML itself.

In a PML, the coordinate system is locally, anisotropically stretched by replacing spatial derivatives $\frac{\partial f}{\partial x}$ in the wave equation by $\frac{1}{1+i\sigma(x)/\omega}\frac{\partial f}{\partial x}$. A complex derivative leads to exponentially decaying solutions wherever $\sigma \neq 0$ causing waves propagating in the PML to attenuate, and leaves the solution unchanged where $\sigma = 0$ so that the PML itself is reflectionless. The angular frequency ω appears to achieve frequency independent attenuation.

Domain Decomposition

Even though the simulated situations are usually in the order of centimeters, compared to typical wavelengths

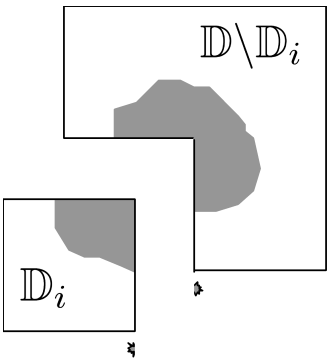

Figure 1: In Domain decomposition, a large domain $\mathbb{D}$ is divided into smaller subdomains $\mathbb{D}_i$ of which the solutions are obtained individually and later recoupled.

$\lambda = 75\mu$m huge volumes have to be discretized. Consequently, large memory loads and computation times are expected, which will have to be limited as much as possible.

Noting that the convolutions in equation (1) are linear operators, the spatial domain $\mathbb{D}$ can be decomposed into smaller subdomains $\mathbb{D}_i$ for $i = 1 \dots N$, of which the solution can be obtained individually. The situation is sketched in Figure 1. However, waves scattering in subdomain $\mathbb{D}_i$ will propagate to the remainder of the domain, $\mathbb{D}\backslash\mathbb{D}_i$. Consequently, the individual subdomains have to be recoupled by computing the convolutions in equation (1) over all subdomains $\mathbb{D}_j$, $j \neq i$, and using the resulting scatter field as an additional incident field. Hence,

$$\widehat{p}^{\,\mathrm{inc}}(\vec{r}) + \widehat{p}^{\,\mathrm{sct}}_{\mathbb{D}\backslash\mathbb{D}_i}(\vec{r}) = \widehat{p}^{\,\mathrm{tot}}(\vec{r}) - \widehat{p}^{\,\mathrm{sct}}_{\mathbb{D}_i}(\vec{r}) \quad (3)$$

where

$$\begin{aligned} \widehat{p}^{\,\mathrm{sct}}_{\mathbb{D}\backslash\mathbb{D}_i}(\vec{r}) &= \widehat{G}(\vec{r},\vec{r}'') * \left[\widehat{k}_0^2 X^\kappa(\vec{r}'')\widehat{p}^{\,\mathrm{tot}}(\vec{r}'')\right] + \\ &+ \widehat{G}(\vec{r},\vec{r}'') * \left[\vec{\nabla}\cdot X^\rho(\vec{r}'')\vec{\nabla}\widehat{p}^{\,\mathrm{tot}}(\vec{r}'')\right] \end{aligned}$$

and

$$\begin{aligned} \widehat{p}^{\,\mathrm{sct}}_{\mathbb{D}_i}(\vec{r}) &= \widehat{G}(\vec{r},\vec{r}') * \left[\widehat{k}_0^2 X^\kappa(\vec{r}')\widehat{p}^{\,\mathrm{tot}}(\vec{r}')\right] + \\ &+ \widehat{G}(\vec{r},\vec{r}') * \left[\vec{\nabla}\cdot X^\rho(\vec{r}')\vec{\nabla}\widehat{p}^{\,\mathrm{tot}}(\vec{r}')\right], \end{aligned}$$

with $\{\vec{r},\vec{r}'\} \in \mathbb{D}_i$ and $\vec{r}'' \in \mathbb{D}\backslash\mathbb{D}_i$. Naturally, this approach requires several iterations through the entire volume, as in the first iteration the total field is not yet known everywhere. Even though this approach increases the computational time, it allows for much larger volumes to be simulated.

Field II

In the Field II software, contrasts are modelled as collections of point scatterers, of which the response can be modelled by an oscillating sphere. The scattered field can then be found by convolving the spatial impulse response of the transducer aperture with the spatial impulse response of these point scatterers. This approach is very efficient in computation time and memory load, and yields accurate results when the Born approximation

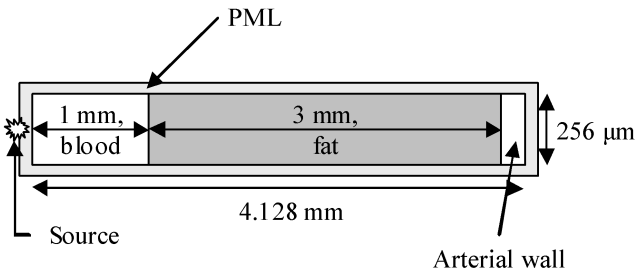

Figure 2: Cross-section of the simulated simplified fatty lesion. Ultrasound is transmitted and received in the same position. For simplicity the simulated 3-dimensional volume is homogeneous in the direction perpendicular to the paper, and has a thickness equal to its height.

is valid. Unfortunately the strength and density of the point scatterers are hard to determine a priori.

Results

To demonstrate the effectiveness of our software, we will compare its output to the output of Field II for a relevant problem in IVUS.

For easy comparison, we chose a simplified model of a section of a fatty atherosclerotic lesion, comprised of blood in the lumen, fat and arterial wall only. The situation is sketched in Figure 2. For simplicity, the intima is neglected and the material properties of the arterial wall are equal to those of the blood, which is approximately true for healthy tissue. The material properties of the different media are given in Table 1.

The height and thickness of the simulated domain are chosen such that reflections off transition layers arrive very localized in time at the transducer. This allows for easy comparison of the arrival times. The excitation pulse is a narrow Gaussian pulse with center frequency of 20 MHz and a temporal sampling rate of 100 MHz is used. The transducer is modeled as a surface of $256 \times 256 \mu m^2$ and located at the position indicated in Figure 2.

The volume element size is $8 \times 8 \times 8 \mu m^3$, resulting in $516 \times 32 \times 32$ elements. This results in a minimum of roughly 4 elements per wavelength at the Nyquist frequency of 50 MHz. Even though this number of elements will fit easily in memory, for illustratory purposes the domain is cut in four equal subdomains in the longest dimension. To avoid the fat region to act as a waveguide, PMLs are

Tissue	Property		
	κ [m^2N^{-1}]	ρ [kg m^{-3}]	c [m s^{-1}]
Blood / Arterial wall	$3.91 \cdot 10^{-10}$	1051	1560
Fat	$4.82 \cdot 10^{-10}$	960	1470

Table 1: Material properties for the simulated tissues. For simplicity the material properties of the arterial wall are set equal to those of blood, which is approximately true for healthy arteries.

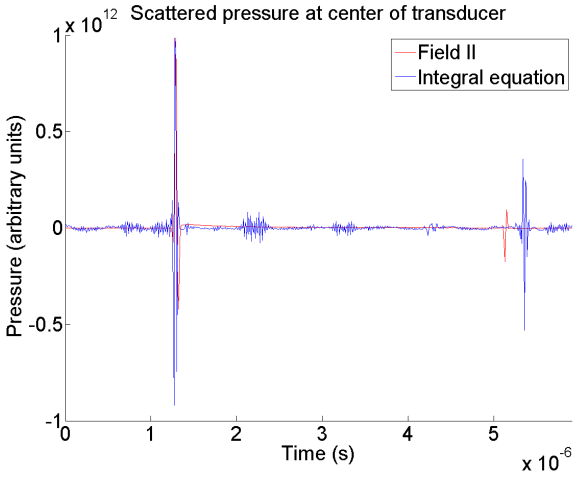

Figure 3: Comparison of the received scattered pressures at the transducer due to scattering off contrasts as defined in Figure 2. There is a clear difference in travel times of the reflection off the end of the fat section.

applied all around the spatial domain.

Due to the simple geometry of the problem it is trivial to predict the shape of the received pressure signal at the center of the transducer. Since there are two contrast interfaces, two sharp peaks are expected of which the arrival times are easily predicted.

The results obtained with both Field II and our code, which solves the scatter integral equation, are shown in Figure 3. From this figure a clear difference between the arrival times obtained with Field II and our code can be observed. The arrival times of the different reflections were read from Figure 3 and the results are given in Table 2.

The arrival times for reflections off the first interface at 1 mm are accurate for both Field II and the integral equation, which indicates that, within their approximations, both methods perform well. As was to be expected, Field II does not yield accurate results for the reflection off the second interface since it operates in the Born approximation. The arrival times obtained with the integral equation approach show good agreement with the predicted values.

Note that the amplitudes of the reflections off the second interface are different for Field II and the integral

Method	Arrival time reflection off interface at	
	1 mm	4 mm
Theory	1.28 μs	5.36 μs
Field II	1.29 μs	5.14 μs
Integral equation	1.28 μs	5.36 μs

Table 2: Arrival times of the two reflections obtained by simulation and those predicted by theory. Note the good agreement with predicted values of the results obtained with the integral equation method, and the difference in results between Field II and the integral equation approach.

equation approach. This is due first to the fact that it is difficult to define accurate scatterer amplitudes in Field II, and second to the Born approximation applied in Field II, as within the Born approximation the incident field is not altered upon scattering. The noise in the plot of Figure 3 remains due to the limited number of iterations through the entire volume.

Conclusions

In this article we have shown that the simulation software Field II in certain cases yields inaccurate results since it operates within the Born approximation. We have presented a method which circumvents the issues associated with the Born approximation by solving, in the temporal Laplace domain, the full scatter integral equation for known incident field, and known contrasts in both compressibility and density. To limit memory usage the computational domain is decomposed into smaller subdomains of which the solutions are obtained individually, and the individual blocks are then recoupled. Perfectly Matched Layers are applied to avoid reflections off the domain boundaries. The numerical results show good agreement with theoretical predictions.

References

[1] Inflammation in Atherosclerosis. Nature **420** (2002), 868-874

[2] Calculation of pressure fields from arbitrarily shaped, apodized, and excited ultrasound transducers. IEEE Trans Ultrason, Ferroelec, Freq Contr **39** (1992), 262-267

[3] Field: A Program for Simulating Ultrasound Systems. Med Biol Eng Comput **34** (1996), 351-353

[4] Two-dimensional multi-level strain estimation for discontinuous tissue. Phys Med Biol **52** (2007), 389-401

[5] The Impact of Physiological Motion on Tissue Tracking During Radiation Force Imaging. Ultrasound Med Biol **33** (2007), 1149-1166

[6] Spatio-Temporal Nonrigid Registration for Ultrasound Cardiac Motion Estimation. IEEE Trans Med Imaging **24** (2005), 1113-1126

[7] Impulse Response Synthesis in Ultrasound Imaging for Vectorial Displacement Estimation. INSA-LYON, Lyon, 2005

[8] Characterization of Carotid Artery Plaques Using Real-time Compound B-mode Ultrasound. Stroke **35** (2004), 870-875

[9] Seismic Applications of Acoustic Reciprocity, Elsevier, Amsterdam, 1993

[10] Bi-CGSTAB: a Fast and Smoothly Converging Variant of Bi-CG for the Solution of Nonsymmetric Linear Systems. SIAM J Sci Stat Comput **13** (1992), 631-644

[11] The Three-Dimensional Weak Form of the Conjugate Gradient FFT Method for Solving Scattering Problems. IEEE Trans Microw Theory Tech **40** (1992) 1757-1766

[12] Notes on Perfectly Matched Layers (PMLs). URL: `http://math.mit.edu/~stevenj/18.369/pml.pdf`